

A Prototype of Ship Routing Decision Support System for an Operational Oceanographic Service

G. Mannarini & G. Coppini

Centro Euro-Mediterraneo sui Cambiamenti Climatici, Lecce, Italy

P. Oddo

Istituto Nazionale di Geofisica e Vulcanologia, Bologna, Italy

N. Pinardi

Università degli Studi di Bologna, Bologna, Italy

ABSTRACT: A prototype for an operational ship routing Decision Support System using time-dependent meteo-oceanographic fields is presented. The control variable is ship course, which is modified using a directional resolution of less than 27 degrees. The shortest path is recovered using a modified Dijkstra's algorithm. Safety restrictions for avoiding surfripping and parametric rolling according to the guidelines of the International Maritime Organization (IMO) are implemented. Numerical experiments tailored on a medium-size vessel are presented and perspectives of development of the system are outlined.

1 INTRODUCTION

A new weather ship routing service is being developed in the framework of European research project IONIO⁵ and Italian industrial research project TESSA⁶. The service will assist the shipmaster in taking decisions for a safe and efficient navigation. The initial Decision Support System (DSS) outlined in this paper will make use of meteo-marine and oceanographic operational information data for all relevant environmental field variables (wind, waves and currents) at high spatial and time resolution. Furthermore, the DSS will provide web-based real-time information.

Academic research in the field of ship routing developed several different approaches, and some of them are briefly reviewed in the following.

Takashima et.al. (2009) propose a method for optimizing fuel consumption. It is based on a

Dijkstra's algorithm for computing the optimal route. The grid is built starting from the standard ship route and adding vertexes on lines perpendicular to the standard route. The authors apply the method to routes along Japan's coast using model environmental forcing with at least 6 miles resolution, and the voyage durations are of the order of one day.

In Wei & Zhou (2012) a dynamic programming method is used in which both ship speed and ship course are control variables. They show that accounting for voluntary ship speed modification leads to extra fuel savings with respect to the optimization with respect to ship course only. Their grid is made up of stages of nodes perpendicular to the great circle. The case study is a route close to the Equator with voyage length of the order of 10 days.

Szłapczyńska & Smierzchalski (2009) perform a multicriteria weather routing optimization with respect to voyage time, fuel consumption, and voyage risk. Their method is based on an evolutionary algorithm. The authors also develop a method of ranking of routes based on the decision-maker's preferences. They apply it to an Atlantic route.

⁵ <http://www.ionioproject.eu/>

⁶ <http://tessa.linksmt.it/>

Montes (2005) provides a detailed documentation of Optimum Track Ship Routing (OTSR), an automation of the weather ship routing service provided by the US navy. The route is retrieved by a binary heap version of Dijkstra’s algorithm. The system employs model fields with $\frac{1}{2}$ degree spatial resolution for both wind and waves in the Western Pacific Ocean. The safety is taken into account by restricting navigation to grid points where wind speed and wave height are within ship’s predefined limits.

For the DSS under development the focus will be on the Mediterranean Sea, where an operational distribution of oceanographic fields is already running⁷ (Pinaridi & Coppini 2010) and subregional models with high spatial temporal resolution are under development in the framework of IONIO and TESSA projects. This will provide a special focus on Southern Italian seas, and in particular on their coastal zone. The prototype DSS illustrated here takes into account the safety restrictions from the most recent technical guidelines for avoiding dangerous situations on the ship. The prototype uses time-dependent environmental information for computation of the optimal route with respect to total navigation time. Route optimization with respect to fuel consumption and other parameters is at the planning stage.

The present paper is organized into 4 sections, which besides Introduction include a description of the structure of the prototype (Sect.2), the application of the prototype to several idealized and yet realistic situations (Sect.3), the conclusions and a brief outlook of future developments (Sect.4).

2 PROTOTYPE STRUCTURE

In this section, the main features of the prototype system application are described: the grid resolution, the input fields, the ship response parametrization, the constraints for navigational safety, and the minimization algorithm.

2.1 Grid

The prototype DSS is based on a shortest path algorithm on a graph.

Graphs are grids for which each gridpoint (“node” or “vertex”) is connected to a subset of the remaining nodes. To each connection (“edge” or “link”) a weight is assigned. If such weight depends on the orientation of the edge, the graph is said to be “directed”. The objective of a shortest path algorithm is to find a sequence of edges between given start and end nodes, which lead to a minimum sum of the weights. If chosen edge weight is the time needed for navigating between edge nodes, then upon termination the shortest path algorithm delivers the minimum voyage time.

Model grid (i.e. the grid on which the meteorological information is available) and graph grid are in general different. Since for the moment we use synthetic data only, we find convenient to identify model and graph grid.

A regular squared grid is constructed, with N_y rows and N_x columns of nodes (see Table 1 for the numerical values of these and other parameters).

In the work of Montes (2005), 8 edges and 8 directions per node are used, corresponding for the northeastern quadrant of origin node O to the nodes marked with A and C in Figure 1. This implies an angular resolution of 45° .

In our prototype instead, each node is connected to a total of 24 edges, allowing for 16 distinct directions. In Figure 1, points marked by A’, B’, C’, and D’ corresponds to the 4 possible directions in the northeastern quadrant of origin node O. Such an organization of the edges enables reaching an angular resolution θ_{12} given by

$$\theta_{12} = \arctan(1/2) \approx 26.6^\circ \quad (1)$$

We deem that in an increase in angular resolution is computationally more effective than an increase in grid resolution obtained by reduction of the intermodal distance. Indeed, doubling the angular resolution ($\theta_{12} \sim 45^\circ/2$) increases the computational cost by a factor of 3 ($=24/8$). Doubling the spatial resolution instead would introduce a factor of 4 ($=2^2$).

Table 1. Parameters of the spatial graph discretization and input field time resolution employed in the prototype.

Symbol	Name	Value	Units
$N_x=N_y$	Linear number of nodes in the spatial grid	30	-
$D_x=D_y$	Spacing of the spatial grid	4	Nautical Miles (NM)
D_t	Time resolution of input fields	1	Hours

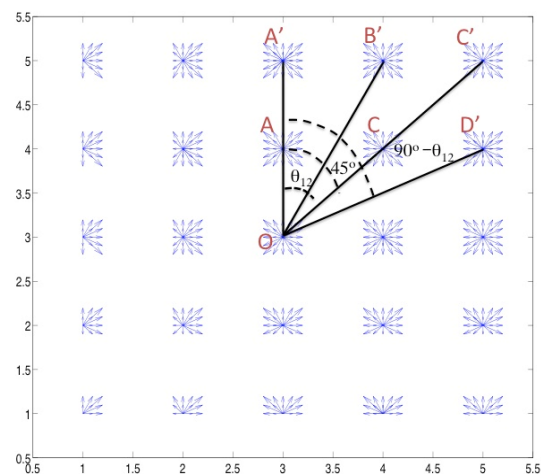


Figure 1. Sample of the plot of graph edges (safegram). At each node, the edges are displayed as arrows pointing to the connected nodes. For clarity, the arrows do not reach the node to which they point. Instead, the edges corresponding to all possible directions in the North-Eastern quadrant of the central node O are drawn as solid lines spanning the whole internodal distance. Note that in the vicinity of the graph border, there are less than 24 edges per node.

⁷ <http://gnoo.bo.ingv.it/myocean/>

Coastline, islands and other types of obstructions can be represented on the grid as polygonal chains, termed “barriers” in the following. Edges containing at least one node laying within or on a barrier are removed from the graph.

2.2 Input fields

Sea state fields taken into consideration are wave height, wave direction, and wave period. At the present stage of development of the prototype, these fields are not yet model output but rather synthetic fields, designed for an idealized testing of the prototype.

Wave height and wave period fields are Gaussian shaped. Allowing peak position of these fields to change with a prescribed velocity generates time-dependent wave height and wave period fields. Time resolution D_t (Table 1) corresponds to the resolution of meteo-marine model fields to be used in the future.

The field of wave direction instead is taken to be homogeneous in space and constant in time.

2.3 Ship response parametrization

The edge weight used is time dt required for navigating between edge nodes, given the involuntary ship speed reduction due to meteo-oceanographic conditions. That is:

$$dt = \frac{dx}{v(\{M\})} \quad (2)$$

where dx is the edge length (Euclidean distance between nodes) and $v(\{M\})$ is the involuntary reduced ship speed due to a set $\{M\}$ of meteo-oceanographic input fields.

For the moment, the effect of wave height and wave direction only is taken into account. Also, voluntary speed reduction is not yet implemented. The motorboat response is parameterized as

$$v(\{M\}) = v(H, \Theta) = v_0 - f(\Theta) \cdot H^2 \quad (3)$$

where H is the significant wave height and Θ is the ship-wave relative direction. Equation 3 is a fit of data displayed in Fig.3703 of Bowditch (2002). The values of coefficient f are reported in Table 2.

Table 2. Values of coefficient f in Equation 3.

	Configuration name	f [kn/ft ²]
$0^\circ \leq \Theta \leq 45^\circ$	Following seas	.0083
$45^\circ < \Theta < 135^\circ$	Beam seas	.0165
$135^\circ \leq \Theta \leq 180^\circ$	Head seas	.0248

By taking into account the added resistance due to the environmental conditions and the ship response operator, a more realistic modelization of ship speed is possible, see e.g. Padhy (2008) and Lloyd (1998). However, such a detail is beyond the purpose of present paper.

We note that, according to Equation 3, edge ship velocity and, consequently, edge weight depends not only on position on the graph but also on direction. Thus, we have a directed graph.

2.4 Safety restrictions

The prototype takes into account some safety restrictions corresponding to the recommendations of the International Maritime Organization (IMO) for avoiding dangerous situations in adverse weather and sea conditions (IMO circular no. 1228). Angle α being the ship-to-wave relative direction ($\alpha=180^\circ$ for following seas), within the prototype it is checked for:

- Surf-riding and broaching-to (shortly termed “surfriding” in this paper). It occurs when both conditions are fulfilled:

$$135^\circ < \alpha < 225^\circ \quad (4.1)$$

$$v_{ship} > \frac{1.8\sqrt{L_{ship}}}{\cos(180^\circ - \alpha)} \quad (4.2)$$

- Parametric rolling motions. It occurs when one of the following conditions is fulfilled:

$$|T_E - T_R| = \varepsilon \times T_R \quad (5.1)$$

$$|2T_E - T_R| = \varepsilon \times T_R \quad (5.2)$$

where the encountered wave frequency $1/T_E$ is Doppler shifted with respect to wave frequency $1/T_w$, as

$$T_E = \frac{3T_w^2}{3T_w + v_{sh} \cos(\alpha)} \quad (6)$$

and ε is the relative tolerance in frequency matching.

Equation 6 holds when wave periods T_E and T_w are expressed in seconds and speed v_{sh} in knots.

In the case that navigation along a given edge leads to a potentially unsafe situation, that edge is removed from the graph. For this reason, we call “safegram” every plot like the one displayed in Figure 1.

2.5 Algorithm

Once the grid and the input fields are correctly prepared, the barrier configuration set up, the ship response provided, and the safety restrictions taken into account, a shortest path algorithm is run to compute the optimal route. A Matlab® implementation of Dijkstra’s algorithm by Joseph Kirk⁸ is used. The edge weight is computed using

⁸ <http://www.mathworks.com/matlabcentral/fileexchange/12850-dijkstras-shortest-path-algorithm>

Equation 2 by evaluating ship velocity through Equation 3 and field values H , Θ at the geometrical meanpoint between edge nodes.

Kirk's routine has been modified in order to recover the shortest path even in presence of time-varying fields. In this case indeed, edge weight is a function of time. In the modified routine, edge weight is evaluated at the time step closest to ship time of arrival at the first node of each edge.

3 RESULTS

Preliminary results obtained using artificial configurations of barriers and synthetic meteo-oceanographic fields are presented.

First, the shortest path in the absence of any input fields is investigated (Section 3.1) and the convergence to the analytical solution is discussed. Then, the effect of safety restrictions according to IMO (IMO circular no. 1228) in the absence of barriers is presented (Section 3.2). Finally, the combined effect of barriers and safety restrictions in presence of forcing fields is computed (Section 3.3).

3.1 Convergence test in the absence of forcing

First, we check the role of space discretization in the computation of the shortest path.

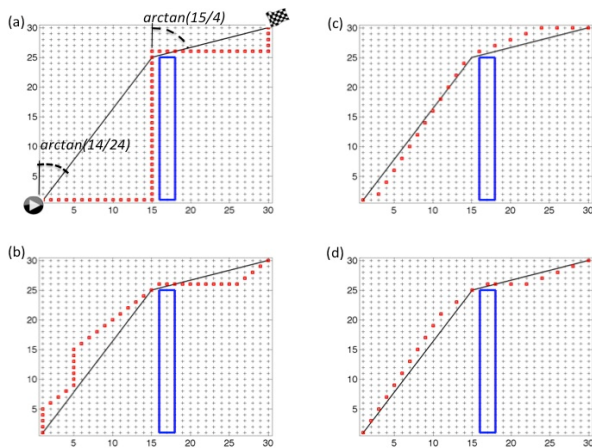


Figure 2. Routes in presence of a barrier (rectangle). Solid lines correspond to the analytical solution, while dots indicate the routes recovered by the algorithm. The panels correspond to different number of edges per node: Respectively 4, 8, 16, 24 for panels a), b), c), d).

We prepare the graph by including a box-shaped barrier and setting to zero all meteo-oceanographic forcing fields (Figure 2.a-d). For this configuration, it is straightforward to find the analytic shortest path. Indeed, it is a polygonal chain which comes as close as possible to the barrier (solid lines in Figure 2.a-d). This implies that the angles formed by the analytical solution with respect to the "meridians" are given by $\arctan(14/24)$ and $\arctan(15/4)$, see Figure 2a. Neither of these angles is permitted by the existing graph edges, as shown by Figure 1. The analytical solution indeed is retrieved when each node is linked to all other nodes (complete graph). Within our graph however, (like in every sparse graph) each node is

connected to a few nodes only. In Figure 2.a-d we display the results of the shortest route computation (dots) for various types of graphs, depending on the number of edges per node. It is seen that, as the number of edges per nodes increases, the computed routes get closer and closer to the analytic solution.

Figure 3 summarizes the results by comparing the lengths of the shortest paths in Figure 2.a-d with the length of the analytic solution. The 24 edges case proposed in this work agrees with the analytic solution within 1.5%, improving by a factor of 5 with respect to the route obtained using the method used e.g. in Montes (2005).

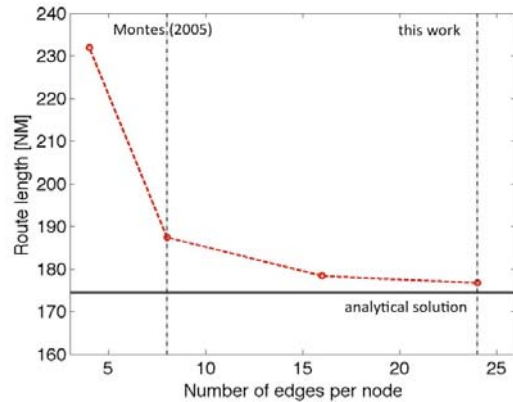


Figure 3. Route lengths for the configurations of Figure 2. The dots correspond to the route lengths in panels (a,b,c,d), while the solid line is the analytical solution.

3.2 Effect of safety restrictions in the absence of barriers

A domain free of any barriers, in which time-dependent sea-state fields are switched on, is now considered. Along all following simulations we strive to use realistic combinations of parameters for both weather and ship modelization.

Some snapshots of the time evolution of significant wave height and wave period field for parameter values given in Table 3 are displayed in Figure 4.

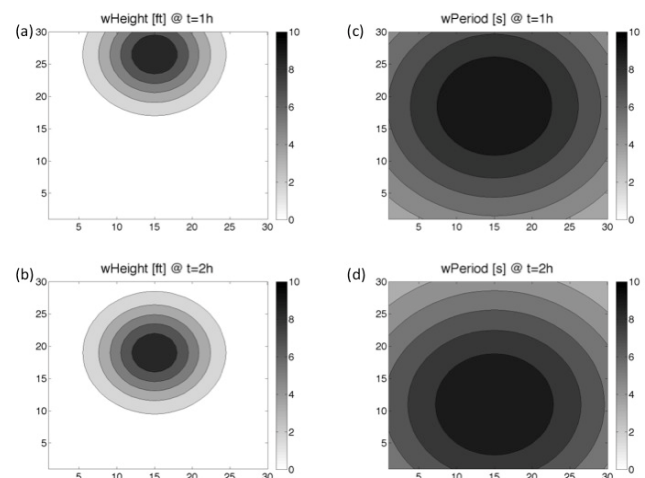


Figure 4. Synthetic significant wave height fields for the surfing experiments (a-b) and wave period fields for the parametric rolling experiments (c-d). For each field, snapshots at the time steps corresponding to 1h and 2h after ship start are shown. Initial positions y_0 are different in the two experiments.

Since sea-state model outputs indicate that wave height and wave period fields are highly correlated⁹, Gaussian synthetic wave period fields with the same peak position of wave height fields are synthesized. However, different peak initial positions y_0 are used in the surfriding and parametric rolling experiments. Wave velocity (knots) is estimated in the deep water approximation, leading to $v_w = 3T_w$ (s), when the fields are expressed in the units given between brackets. Wave direction is always towards the South in our experiments.

Table 3. Weather fields parameters. Values corresponding respectively to the surfriding and parametric-rolling experiments are separated by a semicolon. Wave period parameters are not used in the surfriding experiments.

Parameter name	Symbol	Values	Units
Peak significant wave height	H_{max}	10; 10	ft
Standard deviation of significant wave height	σ_H	20; 20	NM
Peak wave period	T_w	-; 10	s
Standard deviation of Wave peak period	σ_T	-; 64	NM
Wave velocity	V_w	30; 30	kn
Initial (t=0h) peak position	y_0	34; 26	grid-units

Used ship parameters are reported in Table 4. They are chosen in order to mimic a medium size passenger vessel (Ro/Pax).

Furthermore, the side of the simulation domain, $(N_x-1)D_x=116$ NM, is in the range of typical distances for Italy-Greece or Italy-Albania ferryboat routes.

Table 4. Ship parameters. Values corresponding respectively to the surfriding and parametric-rolling experiments are separated by a semicolon.

Parameter name	Symbol	Values	Units
Cruise speed	v_0	19; 18	kn
Length	L_{ship}	100; 100	m
Natural rolling period	T_R	-; 20	s
Tolerance in period matching	ε	-; 10%	-

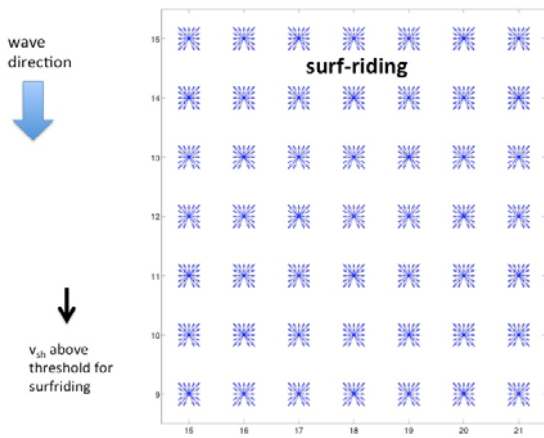


Figure 5. Zoom on the safegram for preventing surfriding and broaching-to at time step 2h after ship start. The peak of the wave field is located in the vicinity of node (15, 15).

⁹ See for instance MFS products at <http://www.sea-conditions.com/en/>

First, we present an experiment set for avoiding surfriding. In Figure 5 it is shown that, for the chosen parameters, accounting for this safety restriction implies avoiding southbound motion. This is due to the fact that the threshold velocity for dangerous motion is lowest for a configuration of following seas ($\alpha=180^\circ$ in Inequality 4.1). The corresponding IMO guideline, Inequality 4.2, does not prescribe a minimum wave height for surfriding to occur, thus, for the chosen ship length L_{ship} and cruise speed v_0 , such a forbidden southbound motion applies to the whole domain.

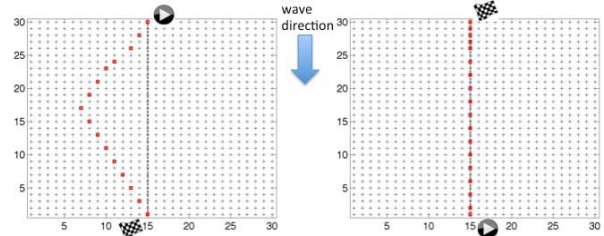


Figure 6. Routes preventing surfriding for a ship leaving a) from the North -navigation time: 7h 03'- and b) from the South -navigation time: 6h 10'- in presence of waves going southwards (dots: safe routes, dashed line: geometrically shortest paths).

The consequences of this structure of the safegram are shown in Figure 6, which shows the time-shortest routes avoiding surfriding, in presence of the forcing due to a wave field moving southwards. In the left (right) panel, a southbound (northbound) ship motion is considered. The southbound motion implies a 32 NM westward diversion, leading to a “knee” in the route. The ship gets at the node corresponding to the knee approximately by the time (+4h) the wave field reaches the southern border of the domain. Instead, the northbound voyage is not affected by the safety restriction and, from the geometrical point of view, it is identical to the straight-line between start and end point. However, the navigation time in the latter case is about 4 minutes longer than the no-weather time (6h 06'). This delay roughly corresponds to the time the ship needs for traversing the wave field with high relative velocity ($v_0+V_w=49$ kn).

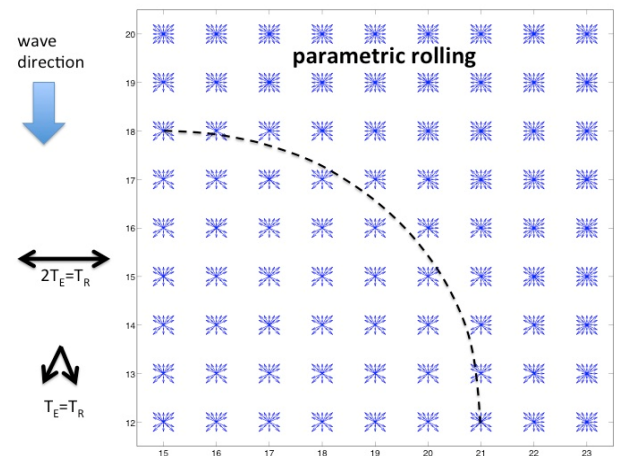


Figure 7. Zoom on the safegram for preventing parametric rolling at time step 2h after ship start. Wave period T_w at the nodes southwestern of the dashed curve is larger or equal to 9 s.

As a second realistic experiment, we set the prototype for simulating a route avoiding parametric rolling. In Figure 7 it is shown that, for the chosen parameters, accounting for this safety restriction implies that several directions are forbidden when the ship is in the vicinity of the wave field. They are $\alpha=\pm 90^\circ$ and $\alpha=180^\circ\pm\theta_2$.

Indeed, for a route at constant latitude, in the present experiment, the wave front is met at 90 degree (beam seas), thus according to Equation 6 there is no Doppler's shift. As a consequence, the Equation 5.2 is fulfilled whenever $2T_W=T_R$, within the prescribed tolerance ε . For the actual parameters, this implies that this condition is fulfilled wherever $T_W=9$ s or larger.

Furthermore, the $T_E=T_R$ condition (Equation 5.1) is fulfilled for $\alpha=180^\circ-\theta_2$ and v_{sh} in the range 15-17 knots which, due to the involuntary ship speed reduction, is also realized within the graph region where $T_W=9$ s or larger.

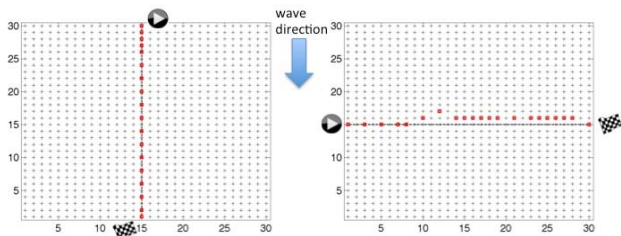


Figure 8. Routes preventing parametric rolling for a ship leaving a) from the North –navigation time: 6h 33'– and b) from the West –navigation time: 6h 41'– in presence of waves going southwards (dots: safe routes, dashed line: geometrically shortest paths).

The consequence of this structure of the safegram are shown in Figure 8, which shows the fastest routes avoiding parametric rolling, in presence of the forcing due to a wave field moving southwards. The southbound route (left panel) is the straight-line between start and end node. The eastbound route (right panel) is affected by the storm beginning from the time the ship gets within the envelope of the $T_W>9$ s area. Since eastbound motion would lead to parametric rolling, at that time step the computed safe route diverts northwards by 8 NM. The diversion leads the ship into a safe region, where parametric rolling is inhibited for all subsequent time steps thanks to the fact that the wavefront moves southwards.

Finally, we investigate a situation in which both environmental forcing and barriers are present. Figure 9 shows a domain with 3 “islands”, set in a way that the narrow channel between the lower 2 islands does not allow a passage with an angle larger than $\arctan(1/3)$ with respect to the meridians. We note that such an angle is smaller than θ_2 defined by Equation 1. Thus, just strictly northbound or southbound ship motions are allowed within the channel. However, the experiment is run checking for the surfriding condition. As we have already seen in Figure 5, this rules out exactly southbound motions. Thus, no safe route can pass throughout the channel. Since passing eastern of the southeastern island would take an even longer time, the route begins as westbound. Thus, we realize that, as a consequence of

a safety restriction, from the very beginning the ship route diverges from the no-weather route.

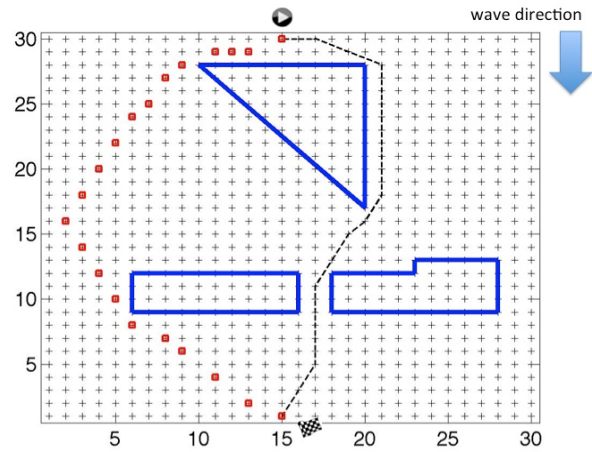


Figure 9. Route preventing surfriding for a ship leaving from the North in presence of waves going southwards and several barriers (dots: safe route –navigation time: 8h 40'; dashed line: geometrically shortest path –navigation time: 7h 23').

3.3 Shortest path in presence of both barriers and safety restrictions.

It is interesting to increase grid resolution and repeat the same experiment, as shown in Figure 10, where $D_x=D_y=2$ NM. The denser spatial grid now allows for a motion through the channel with an angle θ_2 , which is still compliant with the safety restriction. The quality of the resulting route is completely different with respect to the route on the grid with original resolution (its duration is nearly 1h shorter).

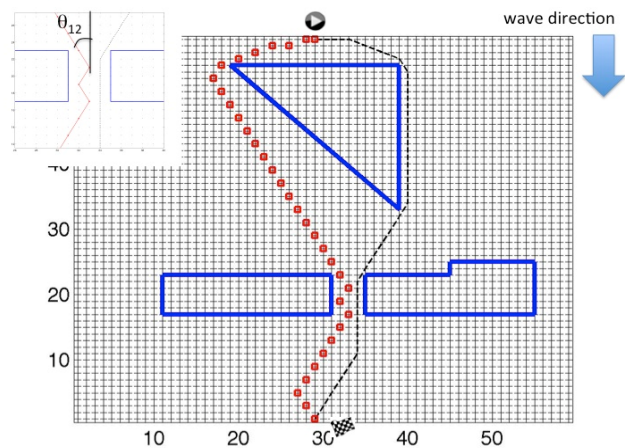


Figure 10. Like Figure 9 but with doubled grid resolution (dots: safe route –navigation time: 7h 42'; dashed line: geometrically shortest path –navigation time: 7h 18'). Inset: zoom on the channel region, showing that the safe route forms an angle θ_2 with the meridians.

Since grid resolution affects ship route, the question arises how to set such a resolution. In our opinion, it is probably not meaningful to increase resolution besides any limit for the sake of allowing sudden course changes. Indeed, real ships have a limited manoeuvrability, and a tight zig-zag motion might be not always possible. Thus, the question on

grid resolution should be answered in the context of a more detailed modelization of ship dynamics.

4 CONCLUSIONS AND OUTLOOK

We have realized a prototype of an automatized ship routing system. The prototype is based on a modified Dijkstra's algorithm for a directed graph. The graph is constructed using 24 edges per node, allowing for an angular resolution of about 27 degrees. The route being shortest in terms of time and safe in the sense of IMO guidances (for preventing surfriding and parametric rolling) is retrieved. The algorithm takes into account time-dependent environmental fields, such as wave height and wave direction. The prototype has been tested in idealized situations, using however realistic combinations of domain-ship-weather parameters.

According to the deliverables of the funding projects IONIO and TESSA, the prototype will evolve into a full DSS for an operational oceanographic service. To this end, several developments of the algorithm and the user interface are planned. Among next steps, we are going to allow for intentional speed reduction as a control variable. Also, route optimization with respect to other parameters, in particular fuel consumption, will be realized. The ship-weather interaction will be modeled in a more realistic way. In particular, along with sea-state fields, also sea currents and sea-surface wind will be used. High spatial and temporal resolution model data for meteorological and oceanographic fields will be employed. Eventually, model data from the Mediterranean Ocean Forecasting System (MFS) will replace the synthetic fields.

ACKNOWLEDGMENTS

Funding through EU-project IONIO and Italian project TESSA is gratefully acknowledged.

REFERENCES

- Bowditch, N. 2002. The American Practical Navigator - an epitome of navigation. *National Imagery and Mapping Agency*.
- International Maritime Organization 2007. Revised guidance to the master for avoiding dangerous situations in adverse weather and sea conditions, *IMO circular no. 1228*
- Krata, P. & Szlapczynska, J. 2012 Weather Hazard Avoidance in modeling safety of motor-driven ship for multicriteria weather routing. *TransNav* vol.6, n.1
- Lloyd, A.R.J.M 1998. Seakeeping – Ship Behaviour in Rough Weather.
- Montes, A.A. 2005. Network shortest path application for optimum track ship routing. *PhD-Thesis, Monterey Naval Postgraduate School*.
- Padhy, C. P. et. al. 2008. Application of wave model for weather routing of ships in the North Indian Ocean. *Nat. Hazards* 44:373–385
- Pinardi, N. and Coppini, G. 2010, Operational oceanography in the Mediterranean Sea: the second stage of development. *Ocean Sci.*, 6, 263-267
- Szlapczynska, J. & Smierzchalski, R. 2009. Multicriteria optimization in weather routing. *TransNav* vol.3, n.4
- Takashima et. al. 2009. On the fuel saving operation for coastal merchant ships using weather routing. *TransNav* vol.3, n.4
- Wei, D. & Zhou, P. 2012. Development of a 3D Dynamic Programming Method for Weather Routing. *TransNav* vol.6, n.1